Supporting Information

Constructing an ultra-absorbent based on porous organic molecule noria for highly efficient adsorption of cationic dyes

Danyong Jiang,[a] Ruiping Deng,[c] Gang Li,[a] Guoli Zheng*[a] and Huadong Guo*[b]

[a]*Key Laboratory of Catalysis and Energy Materials Chemistry of Ministry of Education & Hubei Key Laboratory of Catalysis and Materials Science, South-Central University for Nationalities, Wuhan 430074, China. E-mail: zhengguoli2002@aliyun.com*

[b]*Department of Chemistry, Changchun Normal University, Changchun, 130032, P. R. China. E-mail: hdxmguo@163.com,*

Fax: +86-431-86168210; Tel: +86-431-86168210

[c]*Changchun Institute of Applied Chemistry, Chinese Academy of Sciences 5625 Renmin Street, Changchun, 130022, China*

Adsorption equilibrium

Table S1. Langmuir isotherm model and the Freundlich isotherm model parameters for MB, RhB and NR adsorptions on Noria-POP-1.

Dye	Langmuir model		Freundlich model	
	K_L	R^2	K_F	R^2
MB	3.47×10^{-6}	0.9999	963.5265	0.8339
RhB	1.20×10^{-5}	0.9981	94.0324	0.8498
NR	1.10×10^{-4}	0.9984	180.6606	0.6094

To reveal the adsorption isotherm mechanism. Langmuir and Freundlich eqs were applied to describe adsorption equilibria.

Langmuir equation:

$$\frac{C_e}{Q_e} = \frac{C_e}{Q_m} + \frac{1}{K_l Q_m} \quad (1)$$

Freundlich equation:

$$lnQ_e = lnK_F + \frac{1}{n} lnC_e \quad (2)$$

where Q_e and C_e are defined to be the same as above; K_F ($L \cdot mg^{-1}$) is the Freundlich constant; and n is the heterogeneity factor.

Adsorption kinetics

Table S2. Adsorption kinetic model parameters for MB, RhB and NR adsorption on Noria-POP-1

Dye	Q_e(mg g^{-1})	Pseudo-first-order		Pseudo-second-order	
		K_1 (min^{-1})	R^2	K_2 (g mg^{-1} min^{-1})	R^2
MB	2434	0.983	0.9131	0.1679	0.9992
RhB	855	1.005	0.9566	0.0006	0.9990
NR	590	1.062	0.9562	0.0035	0.9960

The kinetics of MB, NR, and RhB adsorption on Noria-POP-1 were explored using the pseudo-first-order eq 3 and the pseudo-second-order eq 4.

the pseudo-first-order eq 3

$$\frac{1}{Q_t} = \frac{K_1}{Q_e t} + \frac{1}{Q_e} \qquad (3)$$

the pseudo-second-order eq 4

$$\frac{t}{Q_t} = \frac{1}{K_2 Q_e^2} + \frac{t}{Q_e} \qquad (4)$$

where Q_e (mg·g^{-1}) is the adsorption capacity at equilibrium and Q_t (mg·g^{-1}) is the adsorption capacity at time t (min). K_1 (g·mg^{-1}·min^{-1}) is the rate constant of the pseudo-first-ordermodel, and K_2 (g·mg^{-1}·min^{-1}) is the rate constant of the pseudo-second-order model.

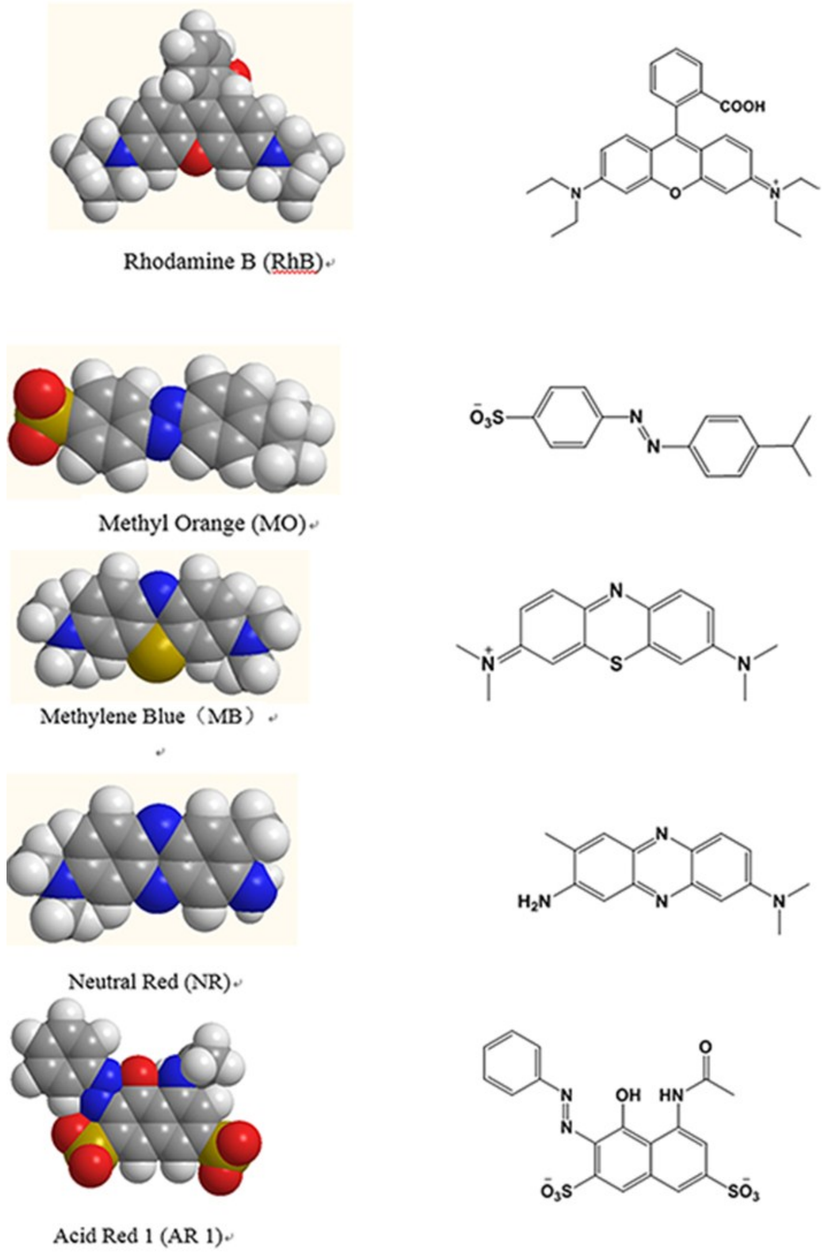

Fig. S1. Molecular structures of MO, AR1, MB, RhB and NR.

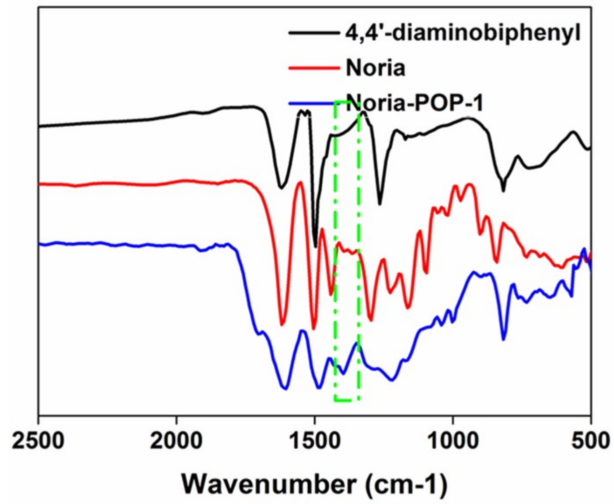

Fig. S2. Fourier transform infrared spectra (FT-IR) of Noria-POP-1; Noria; 4,4'-diaminobiphenyl.

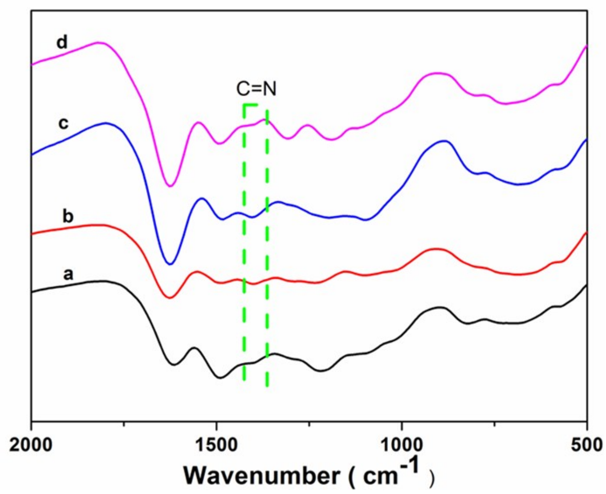

Fig. S3. Fourier transform infrared spectra (FT-IR) of Noria-POP-1(a); MB@Noria-POP-1(b); RhB@ Noria-POP-1(c); NR@ Noria-POP-1(d)

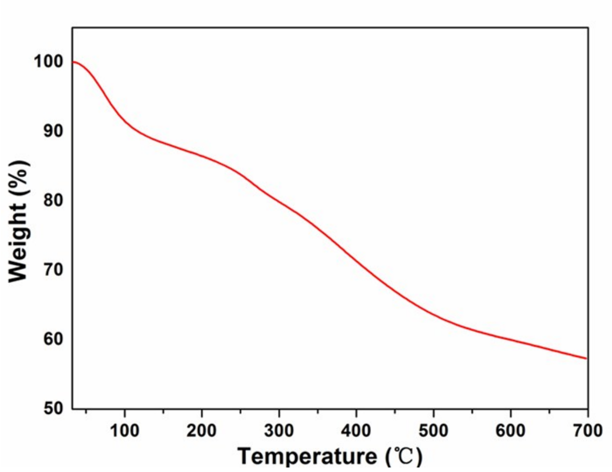

Fig. S4. Thermogravimetric analysis of Noria-POP-1.

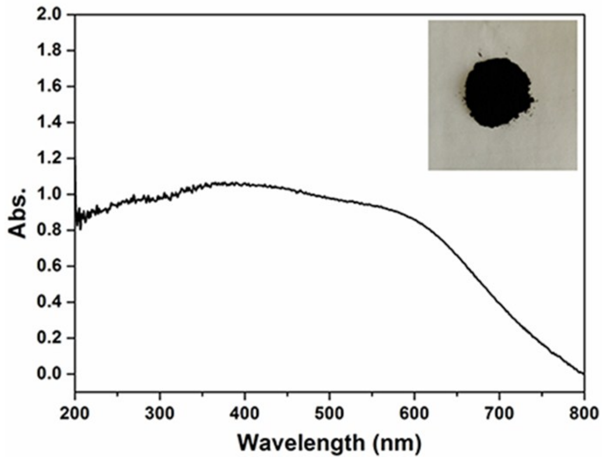

Fig. S5. Ultraviolet absorption spectrum for Noria-POP-1.

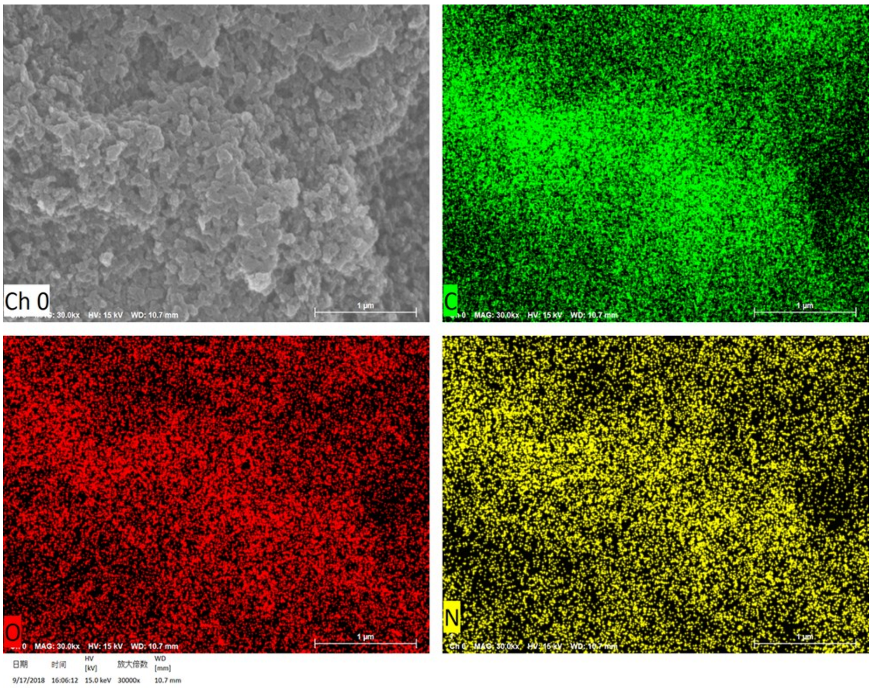

Fig. S6. SEM and EDX images of Noria-POP-1.

Table. S3. Energy dispersive X-ray (EDX) analysis of Noria-POP-1.

Element	Wt %	At %
C	66.515	72.111
N	5.496	5.109
O	27.990	22.780

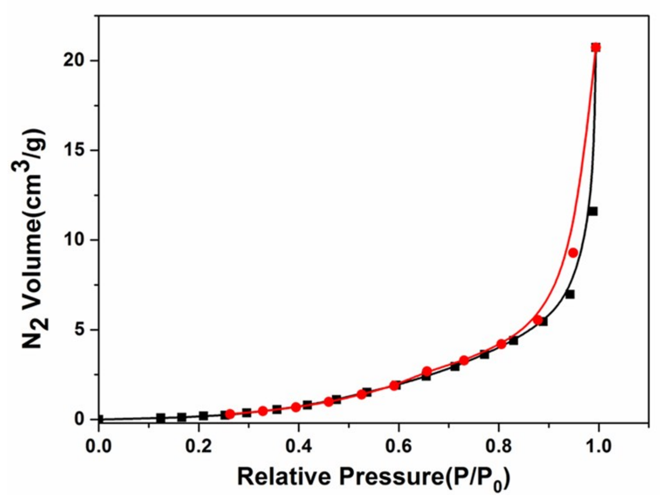

Material	SBET (m^2/g)	Pore volume (cm^3/g)	Pore size (nm)
Noria-POP-1	**1.8**	**0.032**	**70.314**

Fig. S7. N_2 adsorption-desorption isotherms for Noria-POP-1.

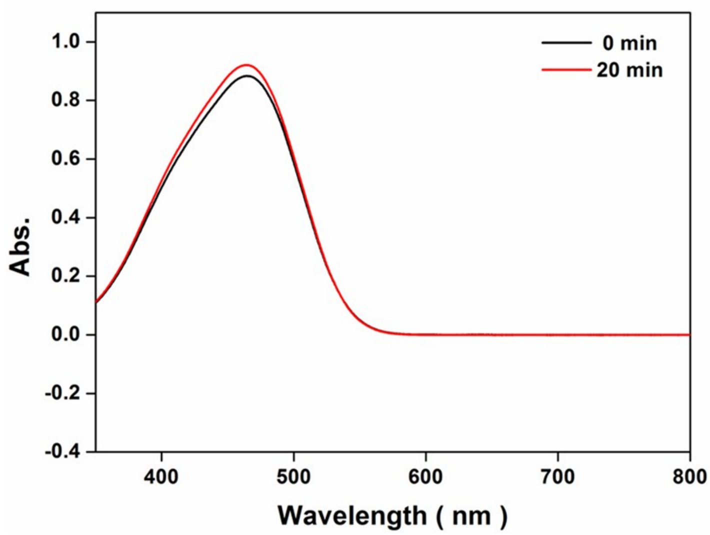

Fig. S8. UV-vis spectra of MO with Noria-POP-1 at given intervals

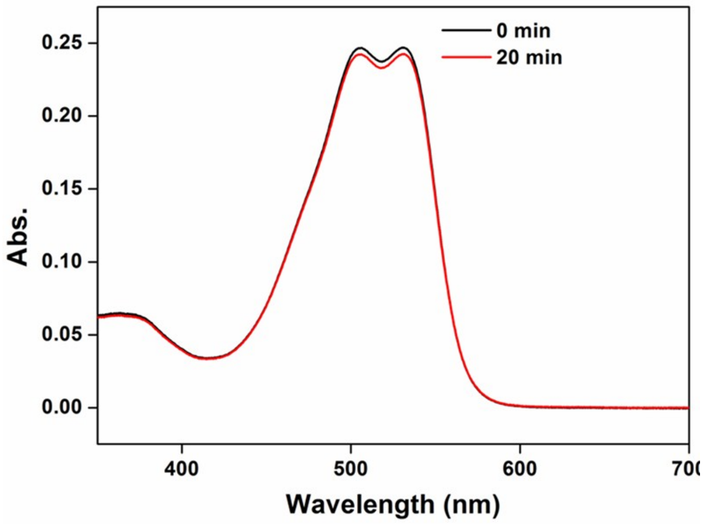

Fig. S9. UV-vis spectra of AR1 with Noria-POP-1 at given intervals

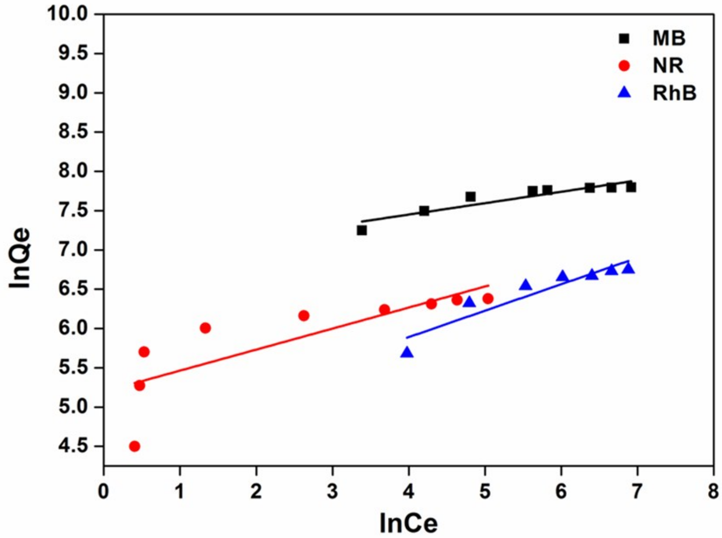

Fig. S10. Freundlich isotherm models of MB, RhB, and NR on Noria-POP-1.

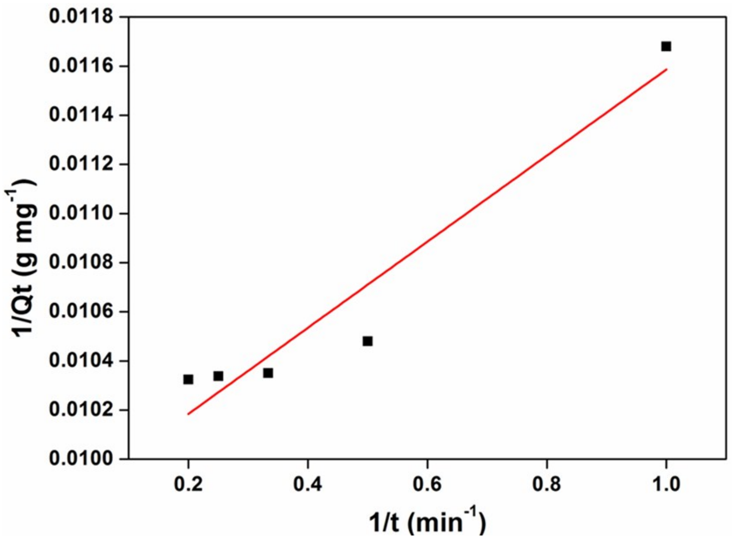

Fig. S11. The pseudo-first-order model of Noria-POP-1 for MB.

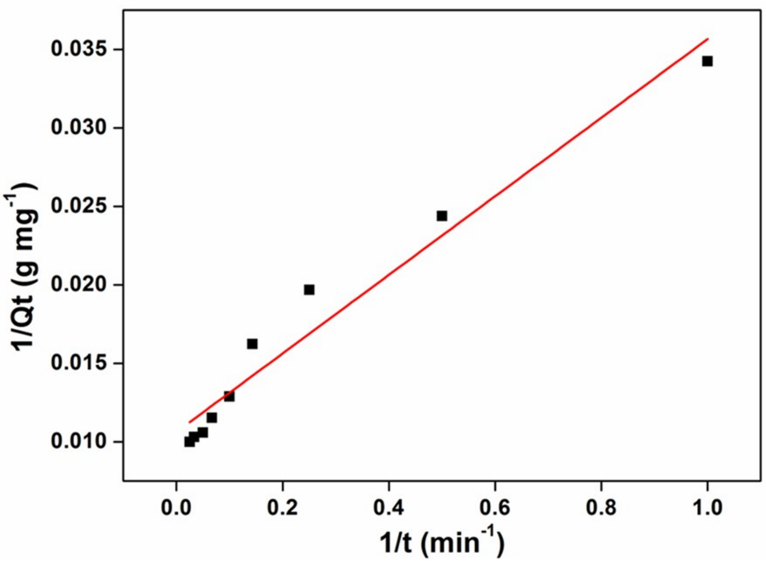

Fig. S12. The pseudo-first-order model of Noria-POP-1 for NR.

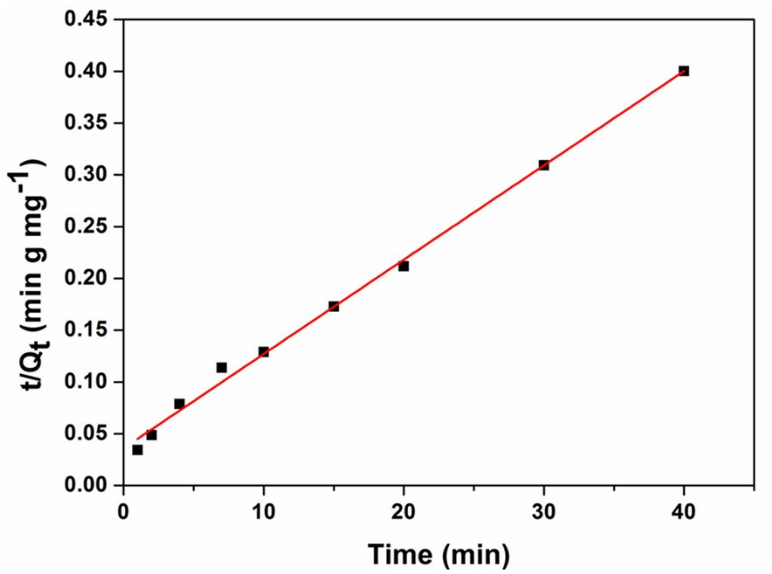

Fig. S13. The pseudo-second-order model of Noria-POP-1 for NR.

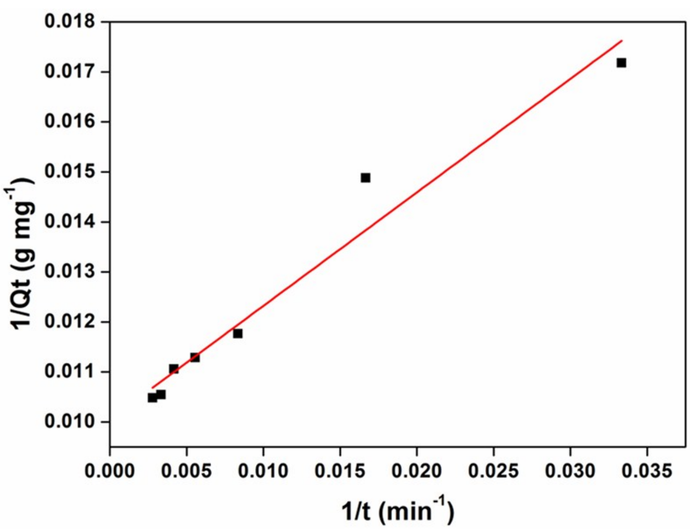

Fig. S14. The pseudo-first-order model of Noria-POP-1 for RhB.

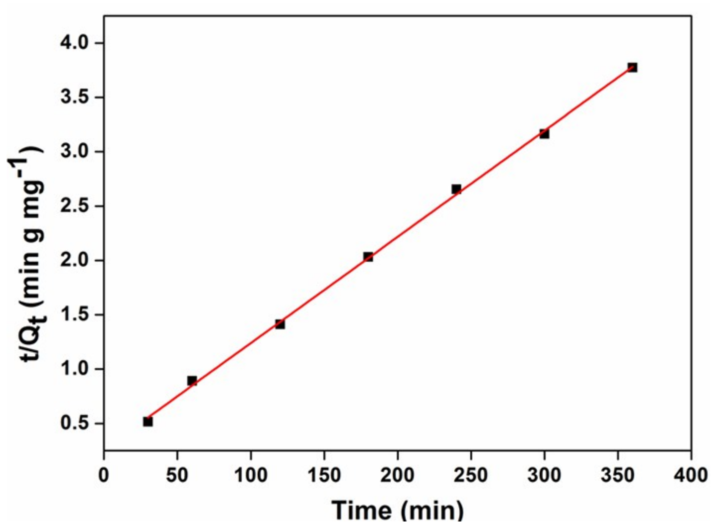

Fig. S15. The pseudo-second-order model of Noria-POP-1 for RhB.

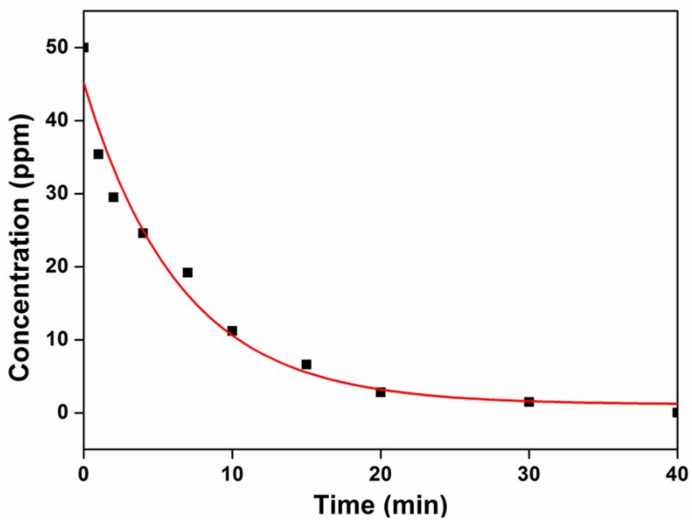

Fig. S16. The effect of contact time on the removal of NR.

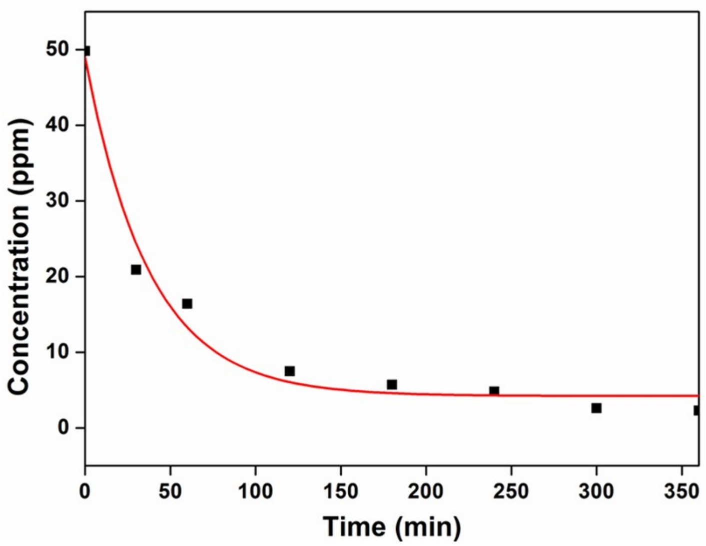

Fig. S17.The effect of contact time on the removal of RhB.

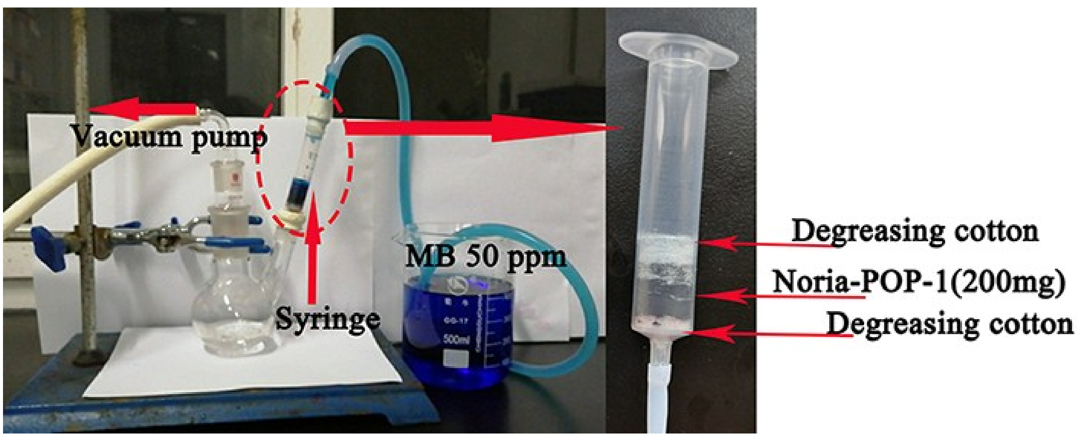

Fig. S18. The adsorption device for MB.

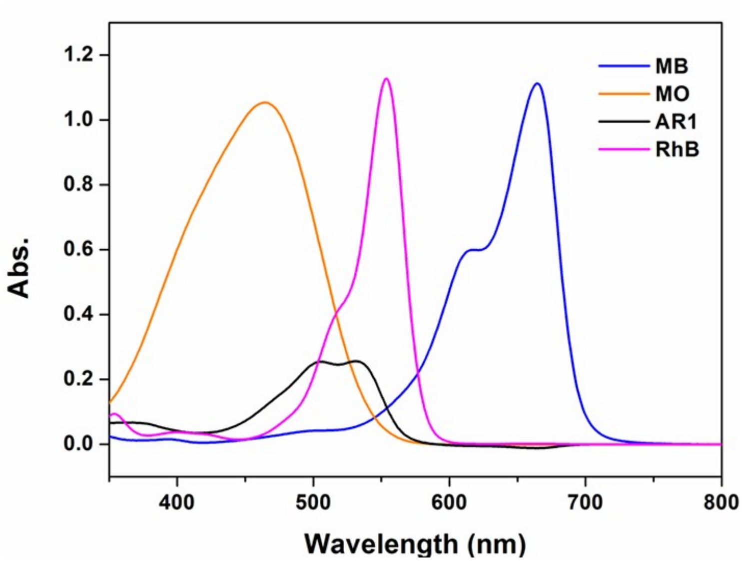

Fig. S19. UV-vis spectra of MO, MB, RhB and AR1.

Table. S4 Comparison of MB adsorption capacity for adsorbents.

Adsorbents	q_{max} (mg g^{-1}) of MB	Ref.
MOP-2	1153	1
TS-COF-1	1691	2
BOPs	3250	3
CaO/g-C3N4	1915.8	4
$[Ca(HDCPP)_2(H_2O)_2]_n(DMF)_{1.5n}$	952	5
ZJU-24	902	6

Porous Carbon sheets	769	7
NH_2-MIL-101(Al)	762	8
Noria-POP-1	2434	This works

References

[1] Huang, L.; He, M.; Chen, B.; Cheng, Q.; Hu, B. Facile Green Synthesis of Magnetic Porous Organic Polymers for Rapid Removal and Separation of Methylene Blue, ACS Sustainable Chem. Eng., 2017, 5,4050−4055.https://doi.org/10.1021/acssuschemeng.7b00031.

[2] Zhu, X.; An, S.; Liu, Y.; Hu, J.; Liu, H.; Tian, C.; Dai, S.; Yang, X.; Wang, H.; Abney, C.W. Efficient Removal of Organic Dye Pollutants Using Covalent Organic Frameworks, AIChE J., 2017, 63, 3470–3478. DOI: 10.1002/aic.15699.

[3] Zhao, X.; Wang, D.; Xiang, C.; Zhang, F.; Liu, L.; Zhou, X. and Zhang, H. Facile Synthesis of Boron Organic Polymers for Efficient Removal and Separation of Methylene Blue, Rhodamine B, and Rhodamine 6G, ACS Sustainable Chem. Eng., 2018, 6, 16777-16787. https://doi.org/10.1021/acssuschemeng.8b04049.

[4] Younis, S. A.; Abd-Elaziz, A.; Hashem, A. I. Utilization of a pyrrole derivative based

antimicrobial functionality impregnated onto CaO/g-C 3 N 4 for dyes adsorption, RSC Adv., 2016, 6, 89367−89379. https://doi.org/10.1039/C6RA10143G.

[5] Hou, Y.; Sun, J.; Zhang, D.; Qi, D.; Jiang, J. Porphyrin–Alkaline Earth MOFs with the Highest Adsorption Capacity for Methylene Blue, Chem. Eur. J., 2016, 22, 6345-6352. https://doi.org/10.1002/chem.201600162.

[6] Zhang, Q.; Yu, J.; Cai, J.; Song, R.; Cui, Y.; Yang, Y.; Chen, B. and Qian, G. A porous metal–organic framework with –COOH groups for highly efficient pollutant removal, Chem. Commun., 2014, 50, 14455-14458. https://doi.org/10.1039/C4CC06648K.

[7] Gong, J.; Liu, J.; Chen, X.; Jiang, Z.; Wen, X. et al. Converting real-world mixed waste plastics into porous carbon nanosheets with excellent performance in the adsorption of an organic dye from wastewater, J. Mater. Chem. A, 2015, 3, 341-351. https://doi.org/10.1039/C4TA05118A.

[8] Haque, E.; Lo, V.; Minett, A. I.; Harris, A. T.; Church, T. L. Dichotomous adsorption behaviour of dyes on an amino-functionalised metal–organic framework, amino-MIL-101(Al), J. Mater. Chem.A , 2014, 2, 193−203. https://doi.org/10.1039/C3TA13589F.